# Transition between viscous and inertial-range scaling of turbulence structure functions

Charles Meneveau
*Department of Mechanical Engineering, The Johns Hopkins University, Baltimore, Maryland 21218*
(Received 7 September 1995; revised manuscript received 11 December 1995)

The transition of velocity structure functions between the viscous and inertial range is examined by assuming a plausible interpolation formula for the required scaling functions. This analysis shows that the recently observed phenomenon of extended self-similarity (ESS) is consistent with assuming that the cutoff length decreases with increasing order of the moment. A revised multifractal formalism is used to quantify this dependence of cutoff scale on the order of the moment. At low and intermediate Reynolds numbers, the proposed mechanism predicts ESS, as well as some additional subtle trends that are experimentally observed. However, at large Reynolds numbers, the shift in cutoff scale predicted by the multifractal formalism becomes too large to be consistent with ESS. [S1063-651X(96)03110-8]

PACS number(s): 47.27.−i

## I. INTRODUCTION

There has been growing (and many would say by now conclusive) evidence that turbulent velocity structure functions [1] of high order

$$\langle(\Delta_r u)^p\rangle \equiv \langle[u(\mathbf{x}+\mathbf{r})-u(\mathbf{x})]^p\rangle \tag{1}$$

deviate from the behavior predicted by the original Kolmogorov 1941 (K41) theory. Above, $u$ is the velocity projected onto the direction of the separation $\mathbf{r}$. The deviation from K41 occurs in the scaling of $\langle(\Delta_r u)^p\rangle$ with separation distance $r=|\mathbf{r}|$, when $r$ is in the inertial range, $\eta \ll r \ll L$ ($\eta=\nu^{3/4}/\langle\epsilon\rangle^{1/4}$ is the Kolmogorov scale, $L$ is the flow's integral scale, and $\langle\epsilon\rangle$ is the mean viscous dissipation rate). For the remainder of this discussion, we shall consider that $u$ is made dimensionless by a large-scale velocity $(\langle\epsilon\rangle L)^{1/3}$. In the inertial range, it has been found experimentally [1,2] and numerically [3] that

$$\langle(\Delta_r u)^p\rangle \sim \left(\frac{r}{L}\right)^{\xi(p)}, \tag{2}$$

where, as $p$ rises, the seemingly universal exponent $\xi(p)$ falls increasingly below $p/3$, the K41 prediction. Summaries of previous work in this area can be found in Refs. [4, 5]. Recent experimental data at very high Reynolds numbers [6] give unambiguous support for deviations from the K41 prediction.

At very small scales, when $r \ll \eta$, the Taylor expansion of $u(x+r)$ yields $\langle(\Delta_r u)^p\rangle \sim r^p$. In recent years there has been growing interest in the behavior of structure functions when the separation distance $r$ transitions from the inertial range [with exponent $\xi(p)$] to the viscous dissipation range (with exponent $p$). This interest has been fueled by the observation of ''extended self-similarity'' (ESS), originally made by Benzi *et al.* [7,4]. They proposed to examine structure functions (defined with an absolute value for reasons of statistical robustness) plotted one versus the other, e.g., $\langle|\Delta_r u|^p\rangle$ versus $\langle|\Delta_r u|^3\rangle$. They found that the range over which the inertial-range exponent $\xi(p)$ is discernible from the logarithmic plots reaches much further into the dissipative range (to about $r_{\mathrm{ESS}} \sim 5\eta$) than for standard scaling with distance [typically $(20–30)\,\eta$]. This effect is practically very advantageous, since standard measurements of $\xi(p)$ inevitably suffer from inaccuracies due to scaling ranges of limited extent, especially at low Reynolds numbers. ESS could thus be used to measure exponents $\xi(p)$ with an unprecedented level of accuracy. The resulting $\xi(p)$ (e.g., reported in [4]—their Table II) confirmed previous results obtained from the traditional method, but at a significantly increased level of confidence. Along a related line of inquiry, we are studying scaling properties of the local subgrid energy flux $\Pi_r(\mathbf{x},t) \equiv -\tau_{ij}\widetilde{S}_{ij}$, where $\tau_{ij}$ is the turbulence subgrid stress tensor at scale $r$ (see, e.g., [8]), and $\widetilde{S}_{ij}$ is the strain-rate tensor, filtered at scale $r$. Using the practice of plotting moments againsts each other (as opposed to scale $r$), we have found very clear scaling properties for moments of $|\Pi_r|$. The results are suggestive of ESS in this context also.

However, an explanation for the phenomenon of ESS is still lacking. Quantitatively, as formulated in [4], one may invoke a scaling function for $p$-order moments $f_p(r/\eta)$, defined as

$$\langle|\Delta_r u|^p\rangle \sim f_p(r/\eta)\left(\frac{r}{L}\right)^{\xi(p)}, \tag{3}$$

where $f_p(x) \to 1$ for $x \gg 1$ and $f_p(x) \to x^{p-\xi(p)}$ for $x \ll 1$. (For consistency with Ref. [4], we use absolute values in the definition of structure functions.) It is simple to show [4] that for $\xi(p)$ scaling of $\langle|\Delta_r u|^p\rangle$ vs $\langle|\Delta_r u|^3\rangle$ to extend to a scale $r_{\mathrm{ESS}}/\eta$, the expression

$$[f_p(r/\eta)]^{1/\xi(p)} \tag{4}$$

must be independent of $p$ down to a scale $r_{\mathrm{ESS}}/\eta$. Such a condition is not easy to satisfy, for we know that for $r \ll r_{\mathrm{ESS}}$ the above expression must depend on $p$ for proper viscous scaling. If one assumes that $f_p(r/\eta)$ depends smoothly on $r/\eta$ and parameter $p$, it becomes difficult to see how $[f_p(r/\eta)]^{1/\xi(p)}$ could be *exactly* independent of $p$ in $r > r_{\mathrm{ESS}}$ while depending on $p$ in $r < r_{\mathrm{ESS}}$. Thus, we suspect that $[f_p(r/\eta)]^{1/\xi(p)}$ is almost (but not exactly) independent of $p$ in the ESS range.

 

In Sec. II, we point out a mechanism that may cause such an approximate collapse. The main argument is given, qualitatively, in Sec. II A. A more quantitative analysis is presented in Sec. III. Finally, a discussion and conclusions are given in Sec. IV.

## II. ANALYSIS

We begin by choosing a particular form for $f_3(r/\eta)$, the scaling function corresponding to the third-order structure function. Batchelor [9] proposed an elegant interpolation formula for the second-order structure function, which has been used recently in several studies (e.g., [10–12]). In Ref. [10], the Batchelor expression was generalized to structure functions of arbitrary order, including proper allowance for intermittency. For the third-order structure function, the proposed expression reads

$$f_3^*(r/\eta)=\frac{1}{[1+(r/\gamma\eta)^{-2}]}. \tag{5}$$

We use $f_3^*(r/\eta)$ [instead of $f_3(r/\eta)$] in order to highlight the possibility that some differences between Eq. (5) and the ''real'' scaling function could exist. With $\gamma\approx 13$, Eq. (5) fits the measured curve reported in Fig. 10 of Ref. [4] quite well. The transition scale $(r/\eta)=\gamma=13$ is in the usually accepted range. Equation (5) smoothly merges the viscous behavior of the structure function $(\sim r^3[1+c_3(r/\eta)^2+\cdots])$ to its inertial range scaling $(\sim r)$. We hasten to point out that, as discussed in detail in Ref. [10], strictly speaking, the above-mentioned viscous behavior can only be derived for structure functions defined without the absolute value. Also, more detailed kinematical relationships relating exponents, velocity derivative moments, and the cutoff scale can be established [10]. Moreover, the Kolmogorov equation provides a dynamical constraint, for relating the scaling function for the second- and third-order structure functions (see Refs. [11, 4]). However, for the present discussion, we continue using the simple form of Eq. (5), mainly because it gives a very good fit through the data of Ref. [4] (their Fig. 10), as well as for other data. But we shall keep in mind that further refinements, such as incorporating the above-mentioned constraints (for formulation without absolute values), are possible.

As proposed in Ref. [10], a possible interpolation formula for $p$-order moments is

$$f_p^*(r/\eta)=\frac{1}{[1+(r/\gamma\eta)^{-2}]^{[p-\xi(p)]/2}}. \tag{6}$$

We defer detailed comparisons with the data of Ref. [4] to a later stage. For now, having selected what may appear at first glance to be a reasonably looking set of scaling functions, we examine the practice of plotting the structure functions against each other, as opposed to the traditional practice of plotting them with respect to scale.

For the sake of further discussion, we also need to prescribe the function $\xi(p)$ with a realistic, but simple, fit. We use the $p$ model [13] and write

$$\xi(p)=1-\log_2(0.7^{p/3}+0.3^{p/3}). \tag{7}$$

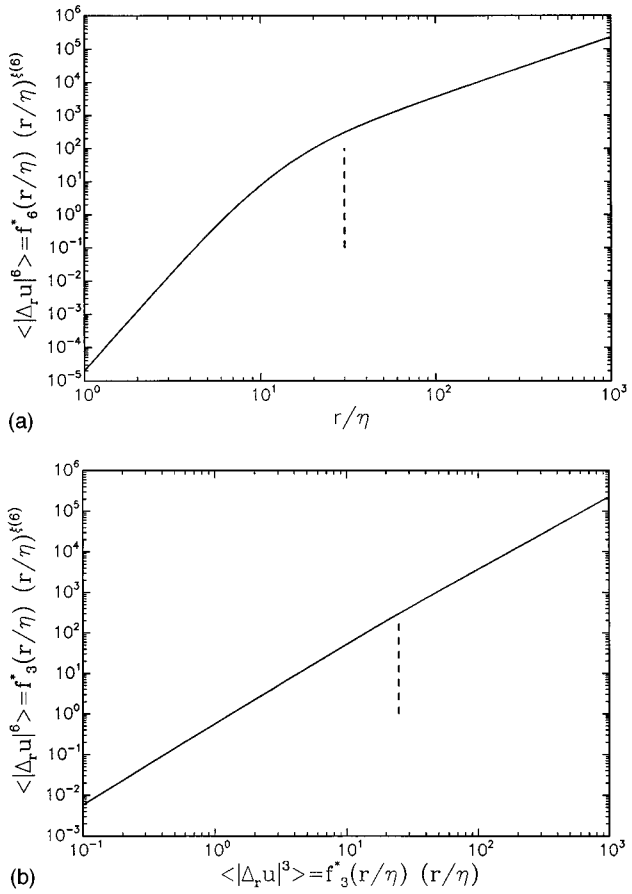


FIG. 1. (a) Traditional log-log plot of hypothetical sixth-order structure function with viscous cutoff [Eq. (6) multiplied by $(r/\eta)^{\xi(6)}$], plotted as a function of distance. The transition between inertial and viscous scaling occurs over an extended range. (b) Alternative log-log plot, in which the hypothetical sixth-order structure function is plotted with respect to the third-order one. The difference between inertial and viscous exponents is much smaller, and the transition occurs in a shorter interval of scales.

We stress that for what follows, any other fit giving reasonable $\xi(p)$ values (such as the log-Poisson model of She and Leveque [14] or the random $\beta$ model [15]) would serve our purposes equally well.

Figures 1(a) and 1(b) show a comparison between plots of hypothetical structure function of order 6,

$$f_6^*(r/\eta)\left(\frac{r}{\eta}\right)^{\xi(6)},$$

plotted in the usual way (versus $r/\eta$) and in the fashion proposed by Benzi *et al.* [7], versus

$$f_3^*(r/\eta)\left(\frac{r}{\eta}\right).$$

The immediate impression is that the scaling in case (b) is much superior compared to case (a). The reason is simply that the transition in (a) occurs between two power laws that are very different [from $\xi(6)\approx 1.76$ to 6 going to small scales] while in case (b) the difference is considerably smaller (from 1.76 to 2). For moments of general order, the

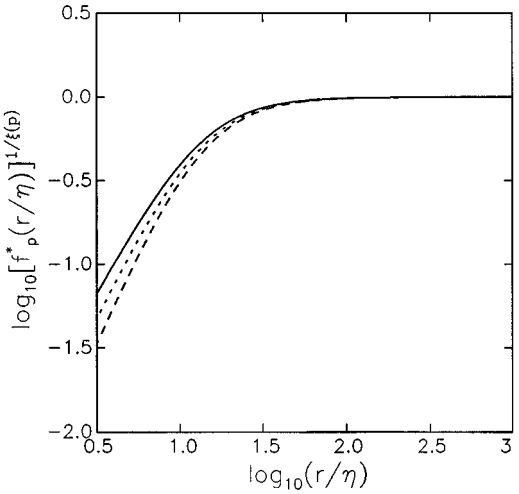


FIG. 2. Hypothetical scaling functions $[f_p^*(r/\eta)]^{1/\xi(p)}$ for $p=2$, 4, and 6 (solid, dotted, and dashed lines, respectively). They are inconsistent with ESS since they already branch out at about $r/\eta\sim 20$.

difference is from $\xi(p)$ to $p$ for scaling with distance, and from $\xi(p)$ to $p/3$ for scaling between structure functions. For such smaller slope differences between two power laws, the extent to which the curving reaches into the power-law region (as measured with respect to some fixed deviation) is shorter, thus allowing for a more accurate determination of the exponents. We conclude that already for this reason alone, the practice proposed in Ref. [7] is advantageous.

Nevertheless, for the example shown in Fig. 1, the scale at which the transition noticeably begins (dashed lines in Fig. 1, at $r=30\eta$), is about the same for both methods [Fig. 1(b) must be viewed edge-on to see this]. On the contrary, the conclusion of extended self-similarity is that the inertial-range scaling between structure functions extends to scales significantly smaller (measurements in Ref. [4] suggest $\sim 5\eta$) than where the curving of the traditional structure function occurs. Thus, while our arguments so far support

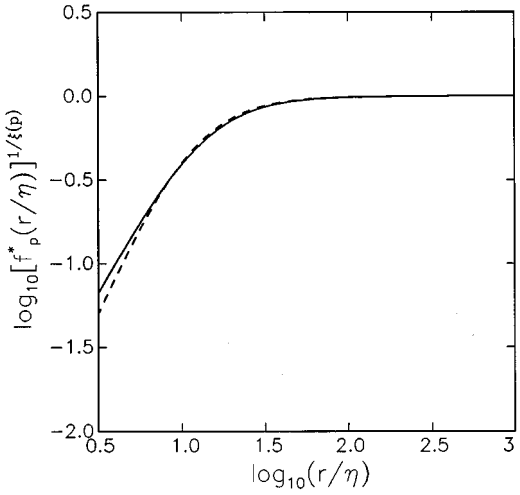


FIG. 3. Comparison between $[f_3^*(r/\eta)]$ and the modified (shifted) curve $[f_6^*(r/0.83\eta)]^{1/\xi(6)}$. This hypothetical situation is consistent with ESS, because the two curves nearly overlap down to $r/\eta\sim 5$.

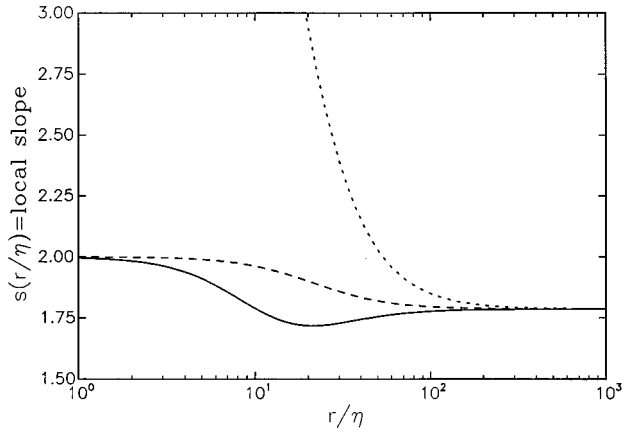


FIG. 4. Comparison of local slopes $s$ (logarithmic derivatives) of sixth-order structure functions, corresponding to several cases. Dotted line is for standard method, $s(r/\eta)=d\{\ln[f_6^*(r/\eta)r^{\xi(6)}]\}/d\ln(r/\eta)$ (extending to 6 at small scales). Dashed line is for scaling with third-order structure function, $s(r/\eta)=d\{\ln[f_6^*(r/\eta)r^{\xi(6)}]\}/d\{\ln[f_3^*(r/\eta)r]\}$. Solid line is for shifted case, $s(r/\eta)=d\{\ln[f_6^*(r/0.83\eta)r^{\xi(6)}]\}/d\{\ln[f_3^*(r/\eta)r]\}$. (Note that the local slopes are plotted as function of $r/\eta$, even though in two of the cases the logarithmic derivatives are not taken with respect to $r/\eta$.)

the rationale for plotting structure functions against each other, they probably have little to do with ESS.

As reviewed in Sec. I a necessary condition for ESS is that $[f_p(r/\eta)]^{1/\xi(p)}$ is independent of $p$, down to a scale $r_{\rm ESS}$ significantly smaller than $30\eta$. Let us now examine to what degree this is the case for our example function $f_p^*(r/\eta)$. In Fig. 2 are plotted $[f_p^*(r/\eta)]^{1/\xi(p)}$ for $p=2,4,6$. The curves branch out to their respective viscous scalings starting near $r/\eta\sim 20$. The curves for high $p$ fall off faster (and thus begin to curve at larger $r$) than those for low $p$, because at small $r$ the function $[f_p^*]^{1/\xi(p)}$ scales as $r^{[p/\xi(p)]-1}$, and the ratio $p/\xi(p)$ increases with $p$ because of intermittency. However, there certainly is no collapse down to $r/\eta\sim 5$, as required by ESS. This figure must be contrasted with the experimentally determined Fig. 8 of Ref. [4], which convincingly shows a much tighter grouping between the different $p$ curves down to about $r\sim 5\eta$.

### A. Main argument

Our central argument can now be made: if the cutoff scale $\eta$ were to slightly decrease with increasing $p$, the high-$p$ curves could possibly move to the left in such a way as to produce a near-collapse of the curves below $r/\eta=20$. For example, imagine that the curve for $p=6$ is translated to the left by an amount $\Delta\log_{10}(r/\eta)\approx 0.08$, i.e., the cutoff scale is multiplied by a factor 0.83. Figure 3 shows the original function $f_3^*(r/\eta)$ for $p=3$, together with the translated curve for $p=6$, namely, $[f_6^*(r/0.83\eta)]^{1/\xi(6)}$. They now fall almost on top of each other, down to significantly smaller values of $r/\eta$ than in Fig. 2. The extended collapse would mean that in the log-log plots between structure functions, inertial-range scaling will be extended to $r/\eta\sim 5$, consistent with ESS. To more clearly exhibit this effect, Fig. 4 shows local slopes (logarithmic derivatives) of the log-log plots of

$f_6^*(r/0.83\eta)r^{\xi(p)}$ vs $f_3^*(r/\eta)r$, as opposed to the unshifted case of $f_6^*(r/\eta)r^{\xi(p)}$ vs $f_3^*(r/\eta)r$. For comparison, we also show the local slopes corresponding to the standard case of $f_6^*(r/\eta)r^{\xi(p)}$ vs $r$, which exhibits the transition from an exponent of $\xi(6)$ to 6 at small scales. The scaling appears worst for this traditional method, and is significantly improved for the scaling with $f_3^*(r/\eta)r$. However, the scaling would appear best for the case in which the $p=6$ curve has been shifted as described above. The small intermediate dip in local slope is unlikely to be seen during analysis of real data, given the typical scatter of empirically determined local slopes.

The observed trend, namely, that an improved collapse occurs when the cutoff scale is shifted, is based here on the Batchelor interpolation formula. While this choice may appear to be rather specific, we would have reached the same qualitative conclusions for any other smooth interpolation formula that is monotonic in both $r$ and $p$, in the sense that $f_p^*(r/\eta)$ is an increasing function of $r/\eta$ for all $p$, and a decreasing function of $p$ for all $r/\eta$.

In summary, we raise the possibility that ESS is due to a $p$-dependent cutoff scale, which happens to shift the curves in the right direction to produce the required ''near-collapse'' of scaling functions in the extended scaling range. In other words, we propose a scaling function of the form

$$f_p(r/\eta)=\frac{1}{[1+(r/\gamma_p\eta)^{-2}]^{[p-\xi(p)]/2}}, \tag{8}$$

essentially the same as $f_p^*(r/\eta)$, except for the fact that the cutoff scale $(\gamma_p\eta)$ now depends on $p$.

The next question that must be answered is whether there exists any *a priori* basis for expecting such a shift of cutoff scale with $p$. Moreover, the shift must depend on $p$ in a particular way, if it is to allow for (approximate) ESS. Multifractality is a possible candidate for such an effect. Indeed, it has been shown [16–19] that within the multifractal formalism of turbulence, stronger events (corresponding to stronger local singularities) are accompanied by smaller local cutoff scales. One may thus qualitatively argue that since higher-order moments are dominated by the stronger singularities, they involve smaller cutoff scales as well. In Sec. III, we describe a plausible quantification of this effect using a refined multifractal formalism.

## III. MULTIFRACTAL FORMALISM WITH TRANSITION TO VISCOUS RANGE

We start by recalling [16–19] that if $\alpha$ is the local singularity strength of one-dimensional (1D) sections through the multifractal dissipation field, as in $\epsilon_r/\langle\epsilon\rangle\sim(r/L)^{\alpha-1}$ [20], the ''local'' Kolmogorov scale follows

$$\frac{\eta(\alpha)}{\eta}\sim\left(\frac{\eta}{L}\right)^{(1-\alpha)/(3+\alpha)}, \tag{9}$$

where $\eta$ is the traditional Kolmogorov scale calculated based on the mean dissipation.

Now we write a local relation for velocity increments

$$|\Delta_r u|\sim g_\alpha[r/\eta(\alpha)]\left(\frac{r}{L}\right)^{\alpha/3}, \tag{10}$$

where the scaling function $g_\alpha[r/\eta(\alpha)]$ is postulated to have the form

$$g_\alpha[r/\eta(\alpha)]=\frac{1}{\{1+[r/\gamma\eta(\alpha)]^{-2}\}^{(1-\alpha/3)/2}}. \tag{11}$$

The scaling function $g_\alpha[r/\eta(\alpha)]$ is such that at $r\ll\eta(\alpha)$, $g_\alpha[r/\eta(\alpha)]\sim[r/\eta(\alpha)]^{1-\alpha/3}$. More importantly, the cutoff scale is allowed to depend on $\alpha$, for the same reason leading to Eq. (9). We remark that the notation of Refs. [21, 15] is recovered by setting $\alpha=3h$.

A digression about Eq. (10) should now be made. Following extensive work of Refs. [22, 23] on locally bridging the velocity-increment and dissipation statistics, one could multiply Eq. (10) (without the absolute values) by a nonintermittent, stochastic variable $V$. This raises the interesting possibility that the observed decrease of the width of probability density functions of $V$ near the viscous range [23] may thus be absorbed in the scaling function $g_\alpha[r/\eta(\alpha)]$. Therefore, writing Eq. (10), instead of $\Delta_r u=V(\epsilon_r r)^{1/3}=V(r/L)^{\alpha/3}$, could render the statistics of $V$ even more universal (independent of local Reynolds number) than they appeared in Ref. [23].

The next step is to describe $P_r(\alpha)$, the probability density of $\alpha$. Again, endowing the usual multifractal formalism with a scaling function, we write

$$P_r(\alpha)=\rho(\alpha)\sqrt{L/r}\;h_\alpha(r/\eta)\left(\frac{r}{L}\right)^{1-f(\alpha)}. \tag{12}$$

The small-scale limit of $h_\alpha(r/\eta)$ is as follows: Since at $r/\eta\ll1$ the $\alpha$ distribution is no longer fractal, the dimension of ''iso-$\alpha$'' sets is 1 (on the 1D sections considered here). Thus $P_r(\alpha)$ no longer depends on the scale $r$, implying $h_\alpha(r/\eta)\sim(r/\eta)^{f(\alpha)-1}$, as $r/\eta\to0$. In analogy with previous scaling functions, we postulate

$$h_\alpha(r/\eta)=\frac{1}{\{1+[r/\gamma\eta(\alpha)]^{-2}\}^{(f(\alpha)-1)/2}}. \tag{13}$$

Next, we proceed to compute the structure functions. As usual, the steepest descent method is employed to evaluate the following integral:

$$\langle|\Delta_r u|^p\rangle=\int_\alpha\left(g_\alpha(r/\eta(\alpha))\left(\frac{r}{L}\right)^{\alpha/3}\right)^p\rho(\alpha)\sqrt{L/r}\;h_\alpha(r/\eta)\times\left(\frac{r}{L}\right)^{1-f(\alpha)}d\alpha. \tag{14}$$

In the limit of large $L/r$, we obtain

$$\langle|\Delta_r u|^p\rangle\sim[g_{\alpha_p}(r/\eta(\alpha_p))]^p h_{\alpha_p}(r/\eta)\left(\frac{r}{L}\right)^{\alpha_p p/3-f(\alpha_p)+1}, \tag{15}$$

where $\alpha_p$ is the $p$-dependent $\alpha$ value at the extremum of the exponent $\alpha p/3-f(\alpha)+1$. This expression is valid for $r$ values such that the scaling functions $g_\alpha$ and $h_\alpha$ are not power laws in $r$. That is, it holds for $r/[\gamma\eta(\alpha)]>O(1)$. In the limit

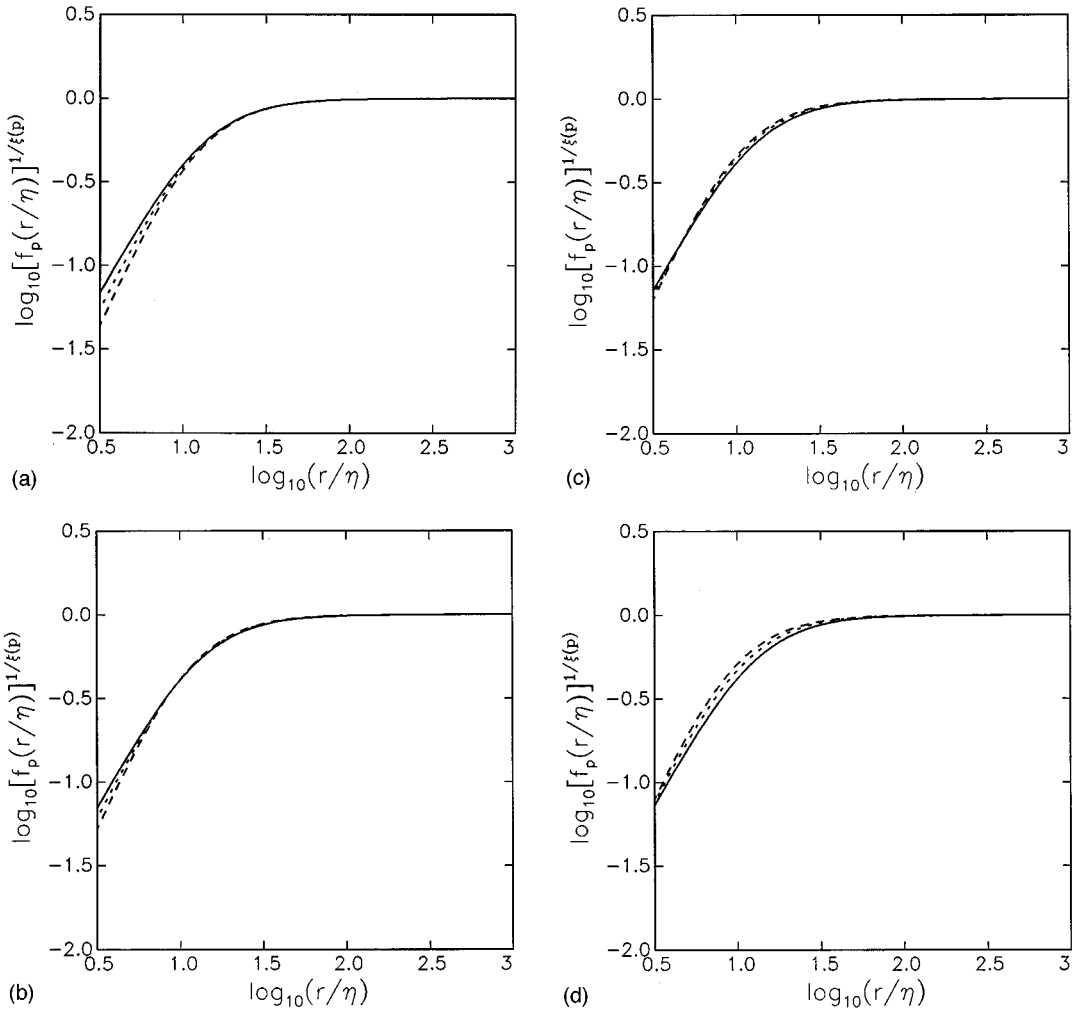


FIG. 5. Scaling functions $[f_p(r/\eta)]^{1/\xi(p)}$ with $p$-dependent cutoff scale [given by Eq. (22)], for $p=2$, 4, and 6 (solid, dotted, and dashed lines, respectively). (a), (b), (c), and (d) correspond to Reynolds numbers $R_\lambda=50$, 100, 200, and 500, respectively.

of $r/[\gamma\eta(\alpha)]\ll 1$, the scaling functions become power laws and their respective exponents must be included in the steepest descent calculation. Such scaling behavior in the very small $r$ limit has been considered by Nelkin [24] in the context of moments of velocity gradients. Since in our current discussion on extended self-similarity, we are interested in the intermediate range $r/[\gamma\eta(\alpha)]\sim O(1)$, Eq. (15) can still be considered valid. Equating with Eq. (3) gives the standard relations among exponents

$$\alpha_p p/3 - f(\alpha_p) + 1 = \xi(p), \tag{16}$$

$$\alpha_p = 3\frac{d\xi(p)}{dp}, \tag{17}$$

but we have the additional condition

$$f_p(r/\eta) = \{g_{\alpha_p}[r/\eta(\alpha_p)]\}^p h_{\alpha_p}(r/\eta). \tag{18}$$

This condition is satisfied as long as

$$(\gamma_p\eta) = \gamma\eta(\alpha_p), \tag{19}$$

or, using Eq. (9),

$$\gamma_p \sim \gamma\left(\frac{\eta}{L}\right)^{(1-\alpha_p)/(3+\alpha_p)}, \tag{20}$$

where

$$\alpha_p = -\frac{0.7^{p/3}\log_2 0.7 + 0.3^{p/3}\log_2 0.3}{0.7^{p/3}+0.3^{p/3}} \tag{21}$$

for the $p$-model parametrization. With this value for the cut off scale $(\gamma_p\eta)$, our proposed expression for $f_p(r/\eta)$ [Eq. (8)] is consistent with the multifractal formalism near the transition between inertial and viscous ranges (but not in the far dissipative range, where the scaling of Nelkin [24] should apply instead).

## IV. DISCUSSION

We now return to our original objective of quantifying the possibility of extended self-similarity. Since Eq. (20) itself is likely to be susceptible to transition behavior when $L/\eta\sim O(10)$, we should replace $(\eta/L)$ by $O(10)(\eta/L)$ in Eq. (20). Arbitrarily, we choose a factor of 10, but the results to be obtained are quite insensitive to this choice, because of

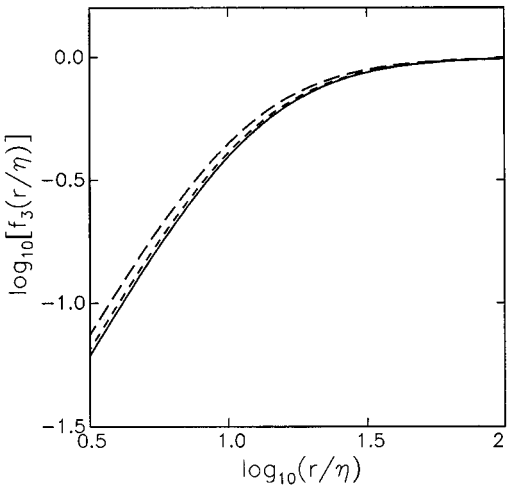


FIG. 6. Reynolds number effect on $f_3(r/\eta)$. Solid line: $R_\lambda=50$, dashed line: $R_\lambda=200$, long dashes: $R_\lambda=800$. Since $(1-\alpha_{p=3})/(3+\alpha_{p=3})\neq 0$, a weak dependence on Reynolds number remains even at fixed $p=3$.

the smallness of the exponent in Eq. (20). For convenience, we express the result in terms of the Taylor-scale Reynolds number $R_\lambda=u'\lambda/\nu$, instead of $L/\eta$. The final expression for the scaling function is

$$f_p(r/\eta)=\left[1+\left(\frac{r}{13\eta}\,(10^{-1}15^{-3/4}\times R_\lambda^{3/2})^{(1-\alpha_p)/(3+\alpha_p)}\right)^{-2}\right]^{[\xi(p)-p]/2}, \qquad (22)$$

valid for $r/(13\eta)>\sim 1$. A weak Reynolds number dependence now appears, as it did (for the case of $p=2$) in the ''intermediate dissipation range'' of Ref. [19], and in recent work on asymptotic scaling of the dissipation rate [25].

Next we explore the behavior of $[f_p(r/\eta)]^{1/\xi(p)}$ within a representative range of Reynolds numbers. Figures 5(a), 5(b), 5(c) and 5(d) show $[f_p(r/\eta)]^{1/\xi(p)}$ for $R_\lambda=50$, 100, 200, and 500, respectively, each containing the cases for $p=2,4,6$. The curves for different $p$ values are quite close to each other (for the low and intermediate Reynolds number cases), down to scales significantly smaller than $20\eta$. It suggests that the multifractal phenomenological picture is consistent with (approximate) ESS in the intermediate range between viscous and inertial scales. More detailed observation [of e.g., Fig. 5(c)] shows the following trend: The $p=6$ line falls slightly above the $p=4$ line for $r>5\eta$, and falls below it for $r<5\eta$ (as it asymptotically must at very small scales). It is interesting to note that a similar crossing behavior is observed in the measured set of curves reported in Fig. 8 of Ref. [4], where the $p=6$ curve (shown with diamonds in their plot) also falls above the $p=2$ curve (squares) at $r<5\eta$, and below the squares at smaller scales. Their $p=4$ curve (triangles) falls in the middle.

For large Reynolds numbers the collapse worsens, because scaling ranges in $r$ become more extended. The displacement of high $p$ curves to smaller scales becomes excessive, with high $p$ lines falling noticeably above the low $p$ ones, down to a crossing scale which decreases with increasing $R_\lambda$. The corresponding logarithmic derivatives (local slopes as in Fig. 4) exhibit an increasingly strong intermediate dip. Thus, the proposed form of Eq. (22) predicts that ESS should weaken at large Reynolds numbers. Of course, in such a case the extended scaling range afforded by ESS is no longer required for accurate determination of inertial-range exponents. Conversely, for very high $p$ values and intermediate $R_\lambda$ values (say $p=15$ and $R_\lambda=200$), the excessive crossing is also observed. It had already been found from data analysis [5] that ESS works less well for the higher-order moments. Nevertheless, we expect this worsening trend to saturate, since the relevant exponent asymptotes to a constant $[(1-\alpha_p)/(3+\alpha_p)\rightarrow 0.14$ as $p\rightarrow\infty]$ from below.

Finally, in Fig. 6, we show $f_3(r/\eta)$ at different Reynolds numbers. If we do not change the moment order, the curves remain quite close, and have the same shape. However, because of the weak $R_\lambda$ dependence in Eq. (22), the curves slightly shift to the left as $R_\lambda$ increases. Examination of Fig. 10 of Ref. [4] shows that a similar trend can be discerned from the experimental data, in which the highest $R_\lambda$ curve (triangles) is shifted to the left (to lower $r/\eta$ values) from the lower $R_\lambda$ curves.

In summary, two main points have been made: (i) ESS can be qualitatively understood if the cutoff scale (in the context of some reasonable interpolation formula) is slightly dependent on the order of the moment, as had been proposed before in the literature [16–19]. (ii) If the multifractal formalism is used to quantify this shift, ESS is recovered for low to moderate Reynolds numbers. Also, some subtle trends of the experimentally obtained scaling functions (such as crossing of curves for different $p$ values and shifts for different Reynolds numbers) are reproduced. This suggests that the proposed mechanism is correct. However, at large Reynolds numbers, the extended scaling in $r$ (or shift in cutoff scale) predicted by the multifractal formalism, becomes large enough to cause an ''overshoot'' when the scaling is viewed according to ESS. To experimentally distinguish between true ESS and the ''overshoot'' predicted from the multifractal formalism will require high Reynolds number data, with high resolution and convergence in the viscous range.

*Note added*. Recently, the author became aware of concurrent work by Benzi *et al.* [26], in which an interpretation of ESS is proposed within the context of ''generalized ESS.''

## ACKNOWLEDGMENTS

The author acknowledges interesting conversations on this topic with G. Stolovitsky, and the comments of M. Nelkin, K. R. Sreenivasan, and R. Benzi. The financial support from NSF (Grant No. CTS9408344) and ONR (Grant No. N00014-92-J-1109) is gratefully acknowledged.

[1] F. Anselmet, Y. Gagne, E. J. Hopfinger, and R. A. Antonia, J. Fluid Mech. **140**, 63 (1984).
[2] Y. Gagne, Ph.D. thesis, Universite de Grenoble, 1989 (unpublished).
[3] A. Vincent and M. Meneguzzi, J. Fluid Mech. **225**, 1 (1991).
[4] R. Benzi, S. Ciliberto, C. Baudet, and G. R. Chavarria, Physica D **80**, 385 (1995).
[5] G. Stolovitzky and K. R. Sreenivasan, Phys. Rev. E **48**, R33 (1993).
[6] F. Belin, P. Tabeling, and H. Willaime, Physica D **93**, 52 (1996).
[7] R. Benzi, S. Ciliberto, R. Tripiccione, C. Baudet, and S. Succi, Phys. Rev. E **48**, R29 (1993).
[8] C. Meneveau, Phys. Fluids **6**, 815 (1994).
[9] G. K. Batchelor, Proc. Cambridge Philos. Soc. **47**, 359 (1951).
[10] G. Stolovitzky, K. R. Sreenivasan, and A. Juneja, Phys. Rev. E **48**, R3217 (1993).
[11] L. Sirovich, V. Yakhot, and L. Smith, Phys. Rev. Lett. **72**, 344 (1994).
[12] D. Lohse, Phys. Rev. Lett. **73**, 3223 (1994).
[13] C. Meneveau and K. R. Sreenivasan, Phys. Rev. Lett. **59**, 1424 (1987).
[14] Z. S. She and E. Leveque, Phys. Rev. Lett. **72**, 1424 (1994).
[15] R. Benzi, G. Paladin, G. Parisi, and A. Vulpiani, J. Phys. A **17**, 3521 (1984).
[16] G. Paladin and A. Vulpiani, Phys. Rep. **156**, 148 (1987).
[17] K. R. Sreenivasan and C. Meneveau, Phys. Rev. A **38**, 6287 (1988).
[18] C. Meneveau and M. Nelkin, Phys. Rev. A **39**, 3732 (1989).
[19] U. Frisch and M. Vergassola, Europhys. Lett. **14**, 439 (1991).
[20] C. Meneveau and K. R. Sreenivasan, J. Fluid Mech. **224**, 429 (1991).
[21] U. Frisch and G. Parisi, *Turbulence and Predictability in Geophysical Fluid Dynamics and Climate Dynamics* (North-Holland, New York, 1985), p. 84.
[22] G. Stolovitzky, P. Kailasnath, and K. R. Sreenivasan, Phys. Rev. Lett. **69**, 1178 (1992).
[23] G. Stolovitzky, Ph.D. thesis, Yale University, 1994 (unpublished).
[24] M. Nelkin, Phys. Rev. A **42**, 7226 (1990).
[25] G. Stolovitzky and K. R. Sreenivasan, Phys. Rev. E **52**, 3242 (1995).
[26] R. Benzi, L. Biferale, S. Ciliberto, M. V. Struglia, and L. Tripiccione (unpublished).